Stress-strain analyses of the jaws with multiple keratocysts before and after surgery

Josef Daněk[1,2], Tatjana Dostálová[3], Milan Hubáček[3], and Nima Mahdian[3]

[1] NTIS – New Technologies for the Information Society, European Centre of Excellence, University of West Bohemia, Univerzitní 22, Pilsen 30614, Czech Republic
[2] Institute of Computer Science, Academy of Sciences of the Czech Republic, Pod Vodárenskou věží 271/2, Prague 18207, Czech Republic
[3] Charles University, 2nd Medical Faculty, Department of Paediatric Stomatology, University Hospital in Motol, V Úvalu 84, Prague 15006, Czech Republic

Abstract. An odontogenic keratocyst was detected and treated in the lower jaw. A 3D reconstruction from a CT scan was made before surgery and 15 months after. The healing process was monitored using stress-strain analyses of the mandible with a system of keratocysts, and by comparing them with the analogous data of stress-strain analyses of the patients mandible after the surgical extirpation of the cysts.

Keywords: Cysts, Dentistry, Gorlin Goltz syndrome

1 Introduction

A 12.5-year-old boy was referred to our clinic by an orthodontist due to right facial asymmetry and accidental X-ray findings (see Fig. 1 revealing large osteolytic lesions on both jaws. A CT scan was done (see Figures 2 and 3). A cystic lesion trespassing from the right ramus of the mandible to the apex of teeth 46 and 47 was found; the germ of the third molar was displaced cranially under the condylar processus. The size of the cystic lesion was 90×45 mm. In localization 18, there was also another noticeable cystic lesion (size 30×20 mm) surrounding the germ of tooth 18, and finally in localization 23, retention and dystopia of tooth 23 was found surrounded by another cystic lesion (size 40×30mm).

The patient had an operation; under general anesthesia an incision was made from localization 47 cranially to the ramus of the mandible. The lifting of the mucoperiostal flap was complicated by the adhesion of the cyst to soft tissues. After the extirpation of the cyst and extraction of the displaced third molar, the neurovascular bundle was clarified. Then, autologous spongious grafts were taken from the right iliac crest and this defect was filled with Surgicel (Ethicon, United Kingdom) and Spongostan (Johnson & Johnson, Czech Rep.). Grafts were ground in a bone mill, the defect in the mandible was augmented using them, and the surgical wound was hermetically closed. Then the mucoperiostal flap was lifted using the intraoral approach in localizations 11 to 24 and the cyst was detected. The cyst was extirpated and tooth 23 was left to spontaneous eruption or bonding and attachment orthodontic bracket and force application in

Fig. 1. OPG X-ray before the surgery: a large cyst of the right ramus of mandible, extending from the apex of tooth 46 cranialy to the colum of the mandible, including the coronoid processus.

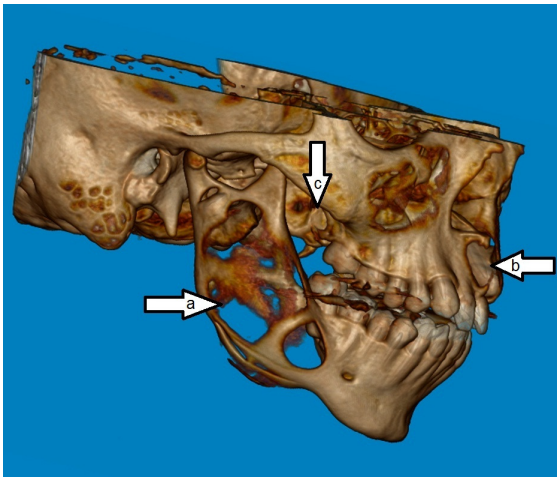

Fig. 2. The CT scan (3D reconstruction) before the surgery: a) the cyst on the right ramus of the mandible with resorption of the lateral and medial compact bones. b) retained tooth 23, surrounded by the cystic lesion. c) resorption of the right tuber of maxilla caused by a cyst in the localization.

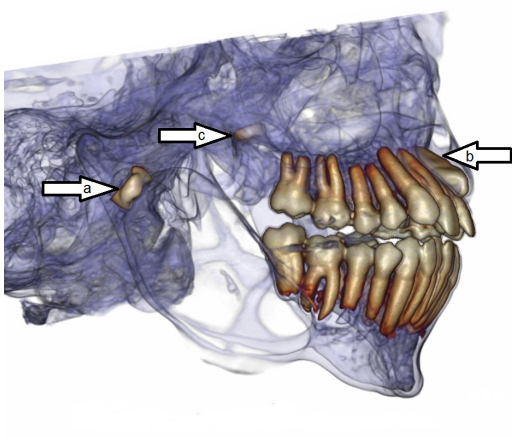

Fig. 3. The CT scan (3D reconstruction) before the surgery: a) the germ of tooth 48 is extruded cranially by the cyst of the mandible. b) retained tooth 23. c) the germ of tooth 18.

the future. Finally, the cyst was extirpated in localization 48 and the germ of 18 was extracted. The recovery proceeded according to plan. However, two months after the surgery, inflammatory complications appeared in the right ramus of the mandible, which were caused by a loss of vitality in tooth 47. The extraction of tooth 47 under local anesthesia and the excochleation of the inflammatory tissues followed. The wound was hermetically sutured, antibiotics were prescribed and it healed without any further complications. 15 months after the surgery, an X-ray and CT scan were done during a checkup (see Figures 4 and 5). We can see that all defects, including the large defect on the right ramus of the mandible, have healed.

Fig. 4. OPG X-ray 15 months after the surgery: healed defect after extirpation of the cyst and extraction of the tooth 47.

A histological examination confirmed the diagnosis of odontogenic keratocysts in all cases. The patient is now in the process of genetic investigation for suspected Gorlin Goltz syndrome because this syndrome involves the principal triad of multiple basal cell nevi, skeletal anomalies and jaw odontogenic keratocysts [4]. An odontogenic keratocyst is a lesion with specific histopathologic features, a high recurrence rate and aggressive behavior [1]. Basal cell carcinomas are locally destructive malignancies of the skin and are the most common type of skin cancer [12].

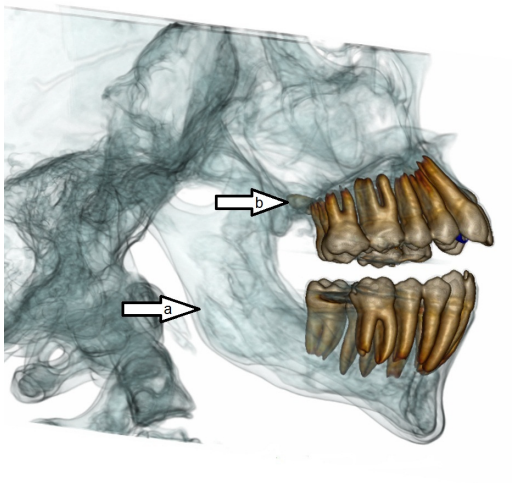

Fig. 5. The CT scan 3D reconstruction 15 months after the surgery. a) healed defect of the mandible after cyst extirpation. b) germ of the tooth 28.

2 Materials and methods

In medical and biological sciences as well as in dentistry, mathematical modeling and mathematical simulation play an important role in the development and progression of bone destruction during the loading of bones [2, 3, 7, 8]. Mathematical modeling is also an invaluable method to help understand the biomechanics of a loaded jaw-bone with cysts in dentistry. The main goal of our study is to obtain data for the stress-strain analyses of the mandible with a system of keratocysts and to compare them with the analogous data of the stress-strain analyses of a patients mandible 15 months after the surgical extirpation of the cysts (see Figures 2 and 3). For the sake of simplicity in our study, we have limited ourselves to studying the mandible with a system of keratocysts only in the first case and the mandible after it has healed in the second case.

In our model, the skull bones are compensated by the choice of useful boundary conditions, which will be discussed later. To model the mandible we first determine its geometry, and secondly, we determine the useful rheology by which we will approximate the biomaterials of the mandible. In our model, for simplicity, we limit ourselves to linear elastic rheology only. Bone is the basic unit of the human skeletal system and provides the framework for and bears the weight of the body, protects the vital organs, supports mechanical movement etc. Based on shape, bones of the skull are flat and for that reason periosteal deposition contributes to the overall growth of those types of bones. Remodeling is a continuous process throughout life, in which damaged bone is repaired, ion homeostasis is maintained, and bone is reinforced for increased stress. In adults, the remodeling rate varies in different types of bones. Trabecular bone is remodeled at a higher rate (25% per year) than that of cortical bone (3% per year) in a healthy adult. Resorption and deposition are normally balanced, and bone density is maintained. A lytic lesion results when resorptive activity exceeds deposition activity in a pathologic state. Bone after cyst formation is not homogenous, the compact cortical bone is harder and trabecular spongious part is destroyed during cyst formation. Based on literature we used for compact bone values of the material parameters E = 1.71×10^{10} Pa, = 0.25 and trabecular spongious was not considered [6, 8, 10].

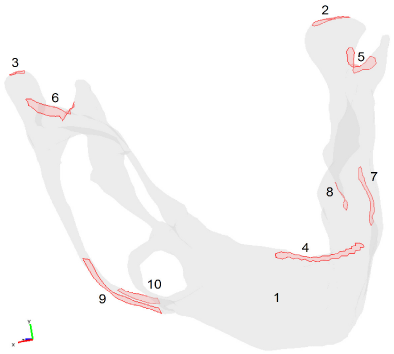

Fig. 6. The surface of TMJ with denoted parts for given boundary conditions (model with cysts).

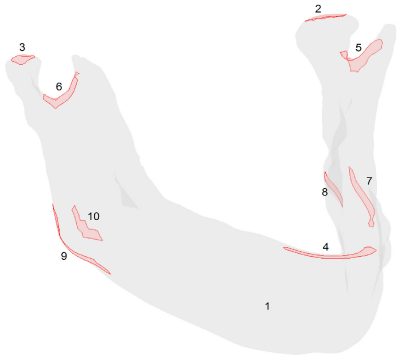

Fig. 7. The surface of TMJ with denoted parts for given boundary conditions (model after the surgery).

Moreover, in our model the skull bones, mainly the bones neighboring the Mandibular fossa, are assumed to be absolutely rigid, and therefore, the possibility for movement of the condyles (heads) in the acetabulae, that is, rotational and translational movements, can be allowed by suitable boundary conditions. Such conditions are the unilateral and bilateral types of conditions. The lengths of the temporal fassae of the skull are limited and the shapes of the temporal

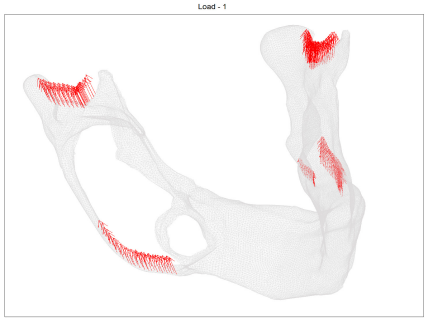

Fig. 8. Prescribed loading for the first case of load for model with cysts.

fossae of the skull are of the special types (the closed jaws, the slightly opened jaws, the widely opened jaws). Since mandibular dislocation occurs when the condyle moves anterior to the articulator eminence, we determine the shapes of the temporal fassae of the skull by using a 3D CT image. Our presented model describes the situation when loaded jaws are closed, the case when the teeth are in mutual contact. During muscular loading, the teeth can move one another and in both acetabulae the condyles can rotate and translate. In our model we simulate these situations by using bilateral contact conditions. Moreover, we assume that in the TMJ, that is, in a synovial lining, synovial fluid is produced, and therefore, we say that the TMJs are synovial types of joints. The synovial fluid acts as a lubricant, and therefore the friction in the TMJs can be omitted. For simplicity, we also assume that the friction on the contact surface between teeth is zero.

The acting muscles: m. Masseter, m. Temporalis, m. Medial pterygoid and m. Lateral pterygoid are denoted by (5)-(10) in Figures 6,7,8, and their magnitudes are given in Table 1 for both models.

Table 1. Boundary conditions - Load 1.

Boundary	1,2,3,4	5	6	7	9	8,10
Face load x-dir. [Pa]	0	-.9e4	.9e4	-.7e4	.7e4	0
Face load y-dir. [Pa]	0	2.8e4	2.8e4	2.4e4	2.4e4	1.5e4
Face load z-dir. [Pa]	0	-.15e4	-.15e4	-.2e4	-.2e4	-.2e4

The 3D reconstruction of the mandible image with the system of keratocysts was obtained on the basis of the CT scan, which was further processed by using the programs Amira and HyperMesh to find the 3D geometry of the mandible. The construction of the model must be based on geometry that is determined with a high level of accuracy. The heads of TMJs are in mutual contact with the skull skeleton during loading (these contact boundaries are denoted by (2) and (3) in Figures 6 and 7). We will assume that the normal displacement components

in contact points are vanishing and that the translation motions are possible only in the tangential planes at the points of the TMJ heads. Since the TMJ heads and glenoid fossa are healthy we will model the temporal bones as absolutely rigid solids and in numerical model we use bilateral condition without friction. The loads are prescribed in the areas where, during occlusion, the Masseter, Temporalis, Medial pterygoid and Lateral pterygoidm muscles (denoted by (5), (6), (7), (8), (9) and (10) in Figures 6 and 7) evoke loading. On the remaining surface of the mandible, the mandible is not loaded, therefore, it can be assumed that this part of the mandibles surface is a free surface without loading.

For our stress-strain analyses, we assume that the working masticatory muscles are characterized by the loading given in Table 1. For the following three cases of loading in both models, we expect an increase of loading in the musculus masseter of about 50%, 100% and 200% (see Figures 6,7,8), under the assumptions that they are less than the tensile strength. For example, the tensile strength of the m. masseter is 0.13 MPa and with increasing age its value decreases [5, 13].

For the realization of a numerical solution, which is based on the theory of semi-coercive unilateral contact problems [8] and the finite element method, COMSOL Multiphysics with the Structural Mechanics Module were used.

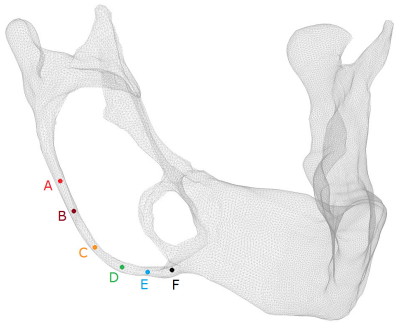

Fig. 9. In the denoted points (A, B, C, D, E and F), we compute the values of the displacements, von Mises stresses and principal stresses (model with cysts).

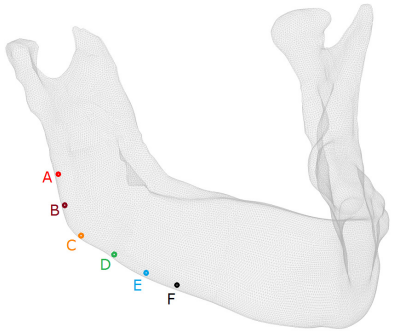

Fig. 10. In the denoted points (A, B, C, D, E and F), we compute the values of the displacements, Von Mises stresses and principal stresses (model after the surgery).

3 Results and discussion

It is obvious that any process which causes resorption or the destruction of bone tissue leads to an increased risk of fracturing the bone. In our case it was a keratocyst, which interfered from the right angle of the mandible through

the ramus of the mandible cranially to the base of the condylar processus. For medical purposes, a 3D mathematical model should be used for verification of the fragile location, where the likelihood of the pathological fracture is most probable.

Table 2. Model I - Total displacement [1e-5 m].

Point	Load 1	Load 2	Load 3	Load 4
A	0.30573	0.42969	0.55437	0.80454
B	**0.44942**	**0.61743**	**0.78562**	**1.12220**
C	0.39630	0.56266	0.72981	1.06497
D	0.28107	0.41318	0.54631	0.81361
E	0.20370	0.27120	0.34011	0.47972
F	0.07307	0.08110	0.09035	0.11129

Table 3. Model I - Von Mises stress [1e5 Pa]

Point	Load 1	Load 2	Load 3	Load 4
A	2.0388	2.9492	3.8640	5.6983
B	2.5311	3.3141	4.1216	5.7693
C	2.6647	2.9209	3.2423	4.0535
D	**4.5392**	**6.2080**	**7.8822**	**11.236**
E	2.8683	4.1153	5.4728	8.3161
F	3.1087	4.6146	6.1383	9.2055

Table 4. Model I - Principal stresses min/max [1e6 Pa]

	Load 1		Load 2		Load 3		Load 4	
Point	min	max	min	max	min	max	min	max
A	-0.2025	0.0049	-0.2921	0.0079	-0.3820	0.0113	-0.5620	0.0185
B	-0.0196	**0.2378**	-0.0350	**0.3048**	-0.0524	**0.3731**	-0.0893	**0.5114**
C	-0.0745	0.2055	-0.0974	0.2120	-0.1229	0.2219	-0.1799	0.2512
D	**-0.4245**	0.0553	**-0.5755**	0.0837	**-0.7269**	0.1125	**-1.0299**	0.1702
E	-0.2832	0.0241	-0.4080	0.0331	-0.5420	0.0442	-0.8209	0.0684
F	-0.3025	0.0168	-0.4551	0.0167	-0.6085	0.0175	-0.9166	0.0203

The finite element mesh is characterized by 48 008 tetrahedrons with 12 265 nodes (for the model with cysts - see Figure 9) and by 70 878 tetrahedrons with 16 801 nodes (for the model after the surgery see Figure 10). In our model we focused on 6 points in the weakest and most stressed areas (see Figures 9 and 10) and compared the measured values before the extirpation of the cysts and

15 months after the surgery. The measured values are listed in the tables above. The changes are very visible in Figures 11 and 12. In the area of weak bone,

Table 5. Model II - Total displacement [1e-5 m].

Point	Load 1	Load 2	Load 3	Load 4
A	0.06394	0.08337	0.10286	0.14190
B	0.06972	0.09272	0.11581	0.16214
C	0.07780	0.10532	0.13292	0.18820
D	0.07444	0.10139	0.12841	0.18254
E	0.06675	0.09101	0.11534	0.16408
F	0.05432	0.07413	0.09401	0.13385

Table 6. Model II - Von Mises stress [1e5 Pa]

Point	Load 1	Load 2	Load 3	Load 4
A	**0.5059**	**0.6568**	**0.8076**	**1.1095**
B	0.2993	0.3964	0.4936	0.6881
C	0.3676	0.5353	0.7040	1.0424
D	0.1786	0.2636	0.3511	0.5285
E	0.2099	0.3053	0.4036	0.6034
F	0.1377	0.1924	0.2485	0.3622

Table 7. Model II - Principal stresses min/max [1e6 Pa]

	Load 1		Load 2		Load 3		Load 4	
Point	min	max	min	max	min	max	min	max
A	**-0.0491**	0.0031	**-0.0638**	0.0038	**-0.0785**	0.0046	**-0.1080**	0.0060
B	-0.0281	0.0029	-0.0372	0.0040	-0.0463	0.0051	-0.0644	0.0072
C	-0.0181	**0.0234**	-0.0249	**0.0354**	-0.0317	**0.0475**	-0.0455	**0.0717**
D	-0.0066	0.0134	-0.0083	0.0209	-0.0102	0.0285	-0.0141	0.0438
E	-0.0152	0.0087	-0.0203	0.0148	-0.0254	0.0210	-0.0359	0.0336
F	-0.0108	0.0047	-0.0143	0.0075	-0.0179	0.0105	-0.0251	0.0164

its deformation is apparent (see Figure 11). This is caused by stress, which is transmitted to this area mainly during mastication. Bone has the ability of slight deformation because of its structure. These include mineral, carbonated hydroxyapatite (also known as dahllite), the framework protein type collagen, many other so-called noncollagenous proteins and water [11]. The collagen included in the bone structure gives it the ability of deformation. For both models and for all cases of loading, we determined the values of total displacement (see Figure

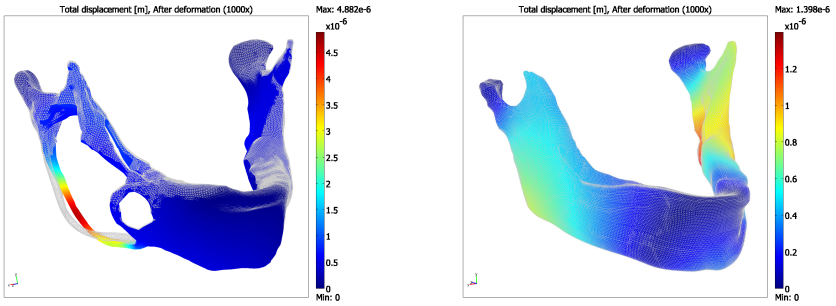

Fig. 11. The total displacement and geometry after deformation (zooming factor 1000) for both models and the first case of load (a) before the surgery, (b) after the surgery.

11 and Table 2 - for the model with cysts, Table 5 - for the model after the surgery), the values of von Mises stresses (see Figure 12 and Table 3 - for the model with cysts, Table 6 for the model after the surgery) and the values of the principal stresses (see Figure 13 and Table 4 - for the model with cysts, Table 7 - for the model after the surgery). In our case, we can see that 15 months after the extirpation of the cysts, the defect has completely healed and the mathematical models confirm this (see Figures 11 and 12).

The negative values of principal stresses in Tables 4 and 7 correspond to the red arrows in Figure 13 and represent the distribution of the pressures in the jawbone. The positive values of principal stresses in Tables 4 and 7 correspond to the blue arrows in Figure 13 and represent the distribution of the tensions in the jaw-bone, which indicate, and moreover, inform us where the jaw-bone is compressed and where it is strained by tension. Moreover, they inform us of which places the jaw-bone can be fractured. Due to the loading of the jaw-bone, stresses accumulate in several places in the jaw-bone. Such places represent singularity-dominated zones in the jaw-bone. These zones can also be the cause of jaw-bone fractures depending on the bone-quality in these zones. By comparing principal stresses computed for dierent loads, we see that the possibility of fractures in a loaded jaw-bone are very probable and inform us about the likely locations of fractures. Our numerical results indicate three areas with higher tensile stresses (see Figure 13a). The tensile stresses in these zones are approximately in the ratio of $1 : 0.91 : 0.59$. From the analyses of the principal stresses and the shear stresses, it is possible to deduce the magnitude of the stresses in these zones. Furthermore, from the analyses of the von Mises stress in these locations, we can deduce the location of possible fracture(s) of a jawbone with keratocysts. Theoretically, these cases are analyzed in [9], where the growth and evolution of cysts are also discussed. The analyses of the jaw-bone after it has healed and been loaded with the same load as in the previous case with the keratocysts, indicate that the behavior of the healed jaw-bone under loading is like a loaded healthy jawbone.

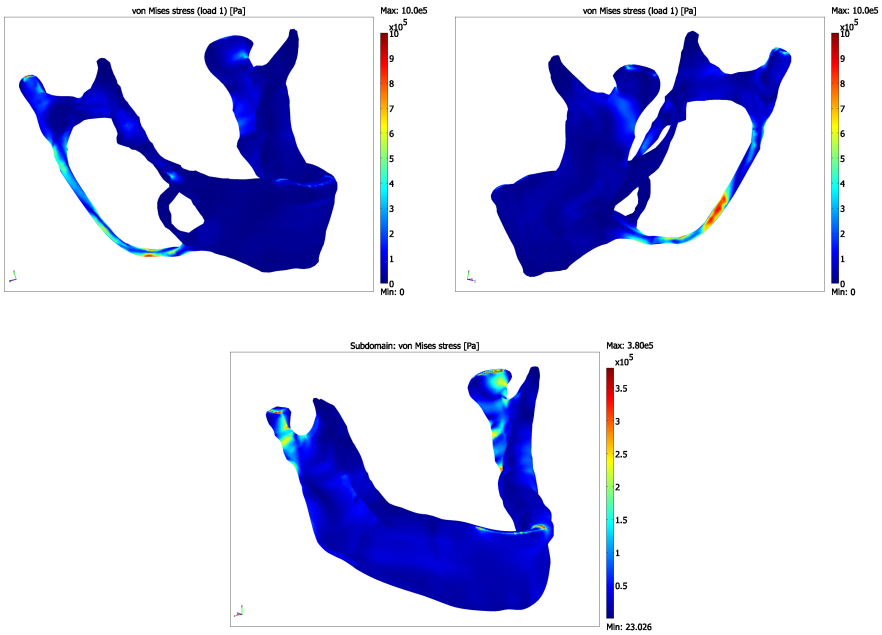

Fig. 12. Von Mises stress for both models and the first case of load (a) right side view for model before the surgery, (b) left side view for model before the surgery, (c) model after the surgery.

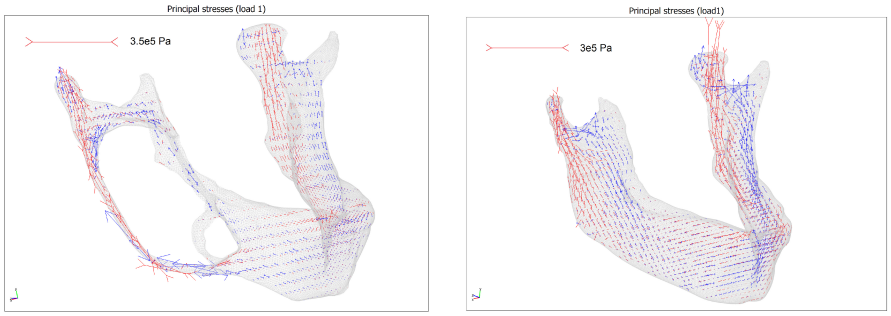

Fig. 13. Principal stresses for both models and the first case of load (a) before the surgery, (b) after the surgery.

Acknowledgements

The paper was supported by the Grant IGA MZCR NT/13351-4.

References

1. Borgonovo A.E., Di Lascia S., Grossi G., Maiorana C.: Twostage treatment protocol of keratocystic odontogenic tumour in zouny patients with GorlinGoltz syndrome: Marsupialization and later enucleation with peripheral ostectomy. A 5-year-follow-up experience. International Journal of Pediatric Otorhinolaryngology 2011 Dec; 75(12): 1565–1571. Epub 2011 Oct 5.
2. Daněk, J., Dostálová, T., Hubáček, M., Mahdian, N., Nedoma, J.: Modeling of the Stress Distribution in Temporomandibular Joint with Subtotal Replacement. In Kim, H.K.; Ao, S.-I.; Amouzegar, M.A.; Rieger, B.B. (Eds.): IAENG Transactions on Engineering Technologies, Lecture Notes in Electrical Engineering, Vol. 247, Springer (2014).
3. Daněk J., Hliňáková P., Přečková P., Dostálová T., Nedoma J., Nagy M.: Modelling of the temporomandibular joints and the role of medical informatics in stomatology. Lecture Notes in Computer Science 6019, pp. 62–71, Springer Vlg., Berlin, Heidelberg 2010.
4. Hegde S., Shetty S.R.: Radiological features of familial Gorlin-Goltz syndrome. Imaging Science in Dentistry, 2012 Mar; 42(1): 55–60. Epub 2012 Mar 22.
5. Katake K.: Studies on the strength of human skeletal muscles. J. Kyoto Pref. Univ. Med. 69, 463, 1961.
6. Natali A.N. (ed.): Dental Biomechanics. Taylor & Francis London and New York 2003.
7. Nedoma J., Stehlík J., Bartoš M., Denk F., Džupa V., Fousek J., et al.: Biomechanics of Human Skeleton and Replacements of Its Parts. Karolinum, Publ. House of the Charles University, Prague, 2006 (in Czech).
8. Nedoma J., Stehlík J., Hlaváček I., Daněk J., Dostálová T., Přečková P.: Mathematical and Computational Methods in Biomechanics of Human Skeletal Systems. An Introduction. Wiley Series in Bioinformatics, John Wiley & Sons, Hoboken, New Jersey 2011.
9. Nedoma J.: Mathematical models of odontogenic cysts and of fractures of jaw-bones. An introductory study. Technical Report No. 1166, ICS AS CR, Prague, 2012.
10. Savoldelli Ch., Bouchard P.O., Loudad R., Baque P., Tillier Y.: Stress distribution in the temporo-mandibular joint discs during jaw closing: a high-resolution three-dimensional finite element model analysis. Surg Radiol Anat (2012) 34:405413.
11. Sharir A., Barak M.M., Shahar R.: Whole bone mechanics and mechanical testing. The Veterinary Journal 177, pp. 817, 2008.
12. Smith V., Walton S.: Treatment of Facial Basal Cell Carcinoma: A Review. Journal of Skin Cancer, Volume 2011, Article ID 380371, 7 pages, doi:10.1155/2011/380371.
13. Yamada H.: In "Strength of Biological Materials" FG Eveans, Ed. The Williams & Wilkins Company, Baltimore, MD 1970.